



Universidad Autónoma
de Madrid

Biblos-e Archivo
Repositorio Institucional UAM

Repositorio Institucional de la Universidad Autónoma de Madrid

<https://repositorio.uam.es>

Esta es la **versión de autor** del artículo publicado en:
This is an **author produced version** of a paper published in:

Journal of Materials Science and Technology 103 (2022):134-143

DOI: <https://doi.org/10.1016/j.jmst.2021.07.004>

Copyright: © 2022 Published by Elsevier Ltd on behalf of The editorial office of Journal of Materials Science & Technology. This manuscript version is made available under the CC-BY-NC-ND 4.0 licence
<http://creativecommons.org/licenses/by-nc-nd/4.0/>

El acceso a la versión del editor puede requerir la suscripción del recurso

Access to the published version may require subscription

Anchoring of 10-phenylphenothiazine to mesoporous silica materials: a water compatible organic photocatalyst for the degradation of pollutants

Daniel González-Muñoz^a, Almudena Gómez-Avilés^b, Carmen B. Molina^b, Jorge Bedia^b,
Carolina Belver^{*,b}, Jose Alemán^{*,a,c} and Silvia Cabrera^{*,d}.

^aOrganic Chemistry Department, Science Faculty, Universidad Autónoma de Madrid, 28049
Madrid, Spain

^bChemical Engineering Department, Science Faculty, Universidad Autónoma de Madrid, 28049
Madrid, Spain

^cInstitute for Advanced Research in Chemical Sciences (IAdChem), Universidad Autónoma de
Madrid, 28049 Madrid, Spain

^dInorganic Chemistry Department, Science Faculty, Universidad Autónoma de Madrid, 28049
Madrid, Spain

*Corresponding authors: silvia.cabrera@uam.es (Silvia Cabrera), jose.aleman@uam.es (Jose Alemán), carolina.belver@uam.es (Carolina Belver)

Keywords: Organic semiconductors; Silica support; Solar photocatalysis; Water treatment; Pharmaceuticals.

Abstract

The application of organic photocatalysts towards the oxidation of pollutants in water is hampered by different limitations such as their insolubility in the media. Herein, we report that the grafting of a photo-organocatalyst into mesoporous silica materials is an ideal approach to obtain effective catalysts. Thereby, the photocatalyst 10-phenylphenothiazine (PTH) was easily anchored into three different mesoporous silica-based materials (MSN, MSU-2 and SBA-15) with different particle sizes and pore sizes through an amide bond formation. The materials were characterized using IR analysis, solid-state X-ray diffraction, porosity and microscopy (SEM and TEM) techniques, showing that PTH is immobilized inside the pores of the materials and its optical properties are maintained after the anchoring. Although homogeneous PTH was inactive in water media, the three photocatalytic materials were active for the degradation of pollutants. SBA-15-AP-PTH exhibited the highest catalytic performance towards the degradation of acetaminophen and diclofenac under solar irradiation, finding in this manner a new strategy for the decontamination of pollutants.

1. Introduction

In last years, photocatalysis has become one of the most popular solutions for the construction of organic molecules [1,2] and the degradation of pollutants [3,4]. Thus, thanks to the energy of the photons provided by solar radiation or light sources (e.g. LEDs), different chemical processes of interest can be carried out. In the field of photocatalysis, the use of phenothiazines has been expanded, encompassing applications such as dye-sensitized solar cells (DSSCs) [5-8], water splitting [9] or hydrogen production [10-15]. More specifically in the organic chemistry field, 10-phenylphenothiazines (PTH) have been employed for the reduction of aryl-halides and oxidation reactions [16], taking

advantage of its high reduction and oxidation potential values ($E_{1/2} = -2.1$ V and $E_{1/2} = 0.75$ V vs SCE, respectively) (Fig. 1A). Moreover, they have been also employed for the synthesis of pharmaceuticals [17], the reduction of allyl derivatives and their functionalization [18], the oxidation of amines into imines [19] and the oxidative cyanation of *N,N*-dimethylaniline [20], among others [21,22]. Despite such unique photocatalytic properties and that they have been successfully used in the synthetic organic chemistry field as photocatalysts, their application in other photocatalytic processes such as the oxidation of pollutants in water purification has not been reported before. In fact, the most common photocatalysts for the oxidative degradation of pollutants are TiO_2 and derivatives [23,24], ternary oxides [25,26], or g- C_3N_4 [27-29], among others [30-33]. By contrast, the use of organic photocatalysts is scarce. One of the main limitations of PTH and related organic photocatalysts to degrade pollutants is their low reactivity and stability in water. Moreover, planar molecules, such as PTH, are also insoluble in many organic solvents and their self-assembly hampers their photocatalytic activity. Because of this, the search for an appropriate platform for anchoring such type of photocatalyst to enhance its photocatalytic performance as well as its solubility would be highly desirable. To the best of our knowledge, this is the first study analysing the PTH anchoring on silica supports as promising photocatalysts for water purification under solar light.

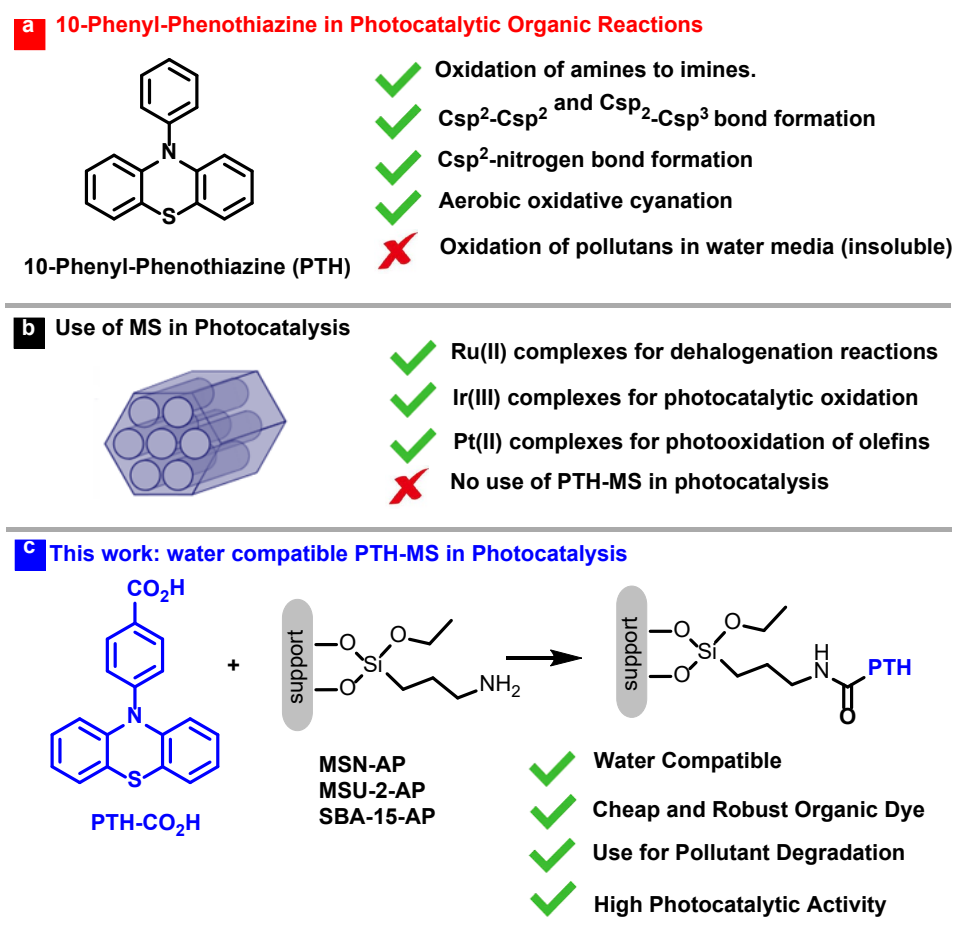


Figure. 1. A) Previous works of PTH in photocatalysis; B) Use of MS in photocatalysis; C) This work: use of PTH-MS in degradation of pollutants.

Mesoporous silica nanoparticles (MS) are a class of materials formed by a SiO₂ matrix, easy to synthesize and functionalize, stable at different temperatures and with tuneable size and pore structure [34-36]. In the last years, MSs have proved to be an outstanding material in which different photocatalysts such as Ru [37], Ir [38], Pt [39-41] and organic molecules [42] have been anchored, showing excellent photocatalytic performance (Fig. 1B). Interestingly, PTH anchored to MS has not been applied yet in photocatalytic processes [43-45]. We envisioned that the covalent bonding of PTH to MS would allow to overcome the disadvantages previously mentioned for being applied as photocatalyst towards the oxidation of pollutants (Fig. 1C). From the catalytic point of view, this approach presents

advantages, such as their compatibility not only with PTH but also with other organic photocatalysts, the local confinement of the catalyst for improving its catalytic activity, the modulation of the properties of the material by using different silicas, the inertness of the MS to the light irradiation, or even the possibility of selective degradation of the pollutant by size or polarity. Herein, we present a new approach for the degradation of pollutants in water using a photocatalytic active organic molecule tethered to different mesoporous silica materials as heterogeneous photocatalyst. Three different silica-based mesoporous materials, namely MSN, MSU-2 and SBA-15, will be studied. All of them present the same chemical composition but different morphology and physical properties. MSNs are spherical particles with hexagonal arrangement of the pores, SBA-15 are elongated spheres with the same type of pores but bigger than those of MSN and, lastly, spherical MSU-2 nanoparticles have wormhole-like arrangement of the pores. The structural differences of the MS supports will allow us to study the influence of their textural and morphological properties into the catalytic performance of the photocatalyst.

2. Experimental

2.1. Chemicals and materials

All chemicals were purchased from commercial sources and were used without further purification. Cetrimonium bromide (CTAB), sodium hydroxide, tetraethyl orthosilicate (TEOS), tris(dibenzylideneacetone)dipalladium ($\text{Pd}_2(\text{dba})_3$), tri-*tert*-butyl phosphonium tetrafluoroborate ($\text{HP}^t\text{Bu}_3\text{BF}_4$), 4-bromobenzonitrile, *N*-hydroxysuccinimide (NHS), *N*-(3-dimethylaminopropyl)-*N'*-ethylcarbodiimide hydrochloride (EDC) and hydroxylamine hydrochloride were purchased from Fluorochem. Potassium hydroxide and sodium *tert*-butoxide (NaO^tBu) were purchased from Acros Organics. Pluronic 123®, tergitol, sodium fluoride, phenothiazine, Celite®, ethyl acetate, cyclohexane, acetic acid, acetaminophen

(ACE), diclofenac (DCF) and phenol (Ph) were purchased from Sigma Aldrich. 2-Mercaptoethanol, toluene and dimethylformamide were purchased from VWR. Dichloromethane and ethanol were purchased from Fisher Chemicals. Hydrochloric acid (35-38% aq. solution) was purchased from LabKem. Acetonitrile (HPLC grade) was purchased from Scharlab. The synthesis of MSN [46], SBA-15 [47] and MSU-2 [48] materials and their aminopropyl-functionalized materials [49] were carried out following literature procedures. The detailed procedures are described in Supplementary Material.

2.2. Synthesis of 4-(10H-phenothiazin-10-yl)benzoic acid (PTH-COOH)

2.2.1. Synthesis of PTH-CN

The synthesis of PTH-CN was performed following a previous work [50,51] (see Scheme 1). Phenothiazine (1.83 g, 10.0 mmol), *p*-bromobenzonitrile (2.00 g, 11.0 mmol), Pd₂(dba)₃ (275.0 mg, 0.3 mmol) and HP^tBu₃BF₄ (145.0 mg, 0.5 mmol) were added to a sealed tube. Then, 11 mL of toluene were added and the mixture was stirred for 15 min. Finally, NaO^tBu (1.11 g, 11.5 mmol) was added and the reaction mixture was stirred at 110 °C for 48 h. After cooling to room temperature, the resulting mixture was diluted with dichloromethane (20 mL) and filtered through a pad of Celite®. The celite pad was washed with dichloromethane (4 x 10 mL) and the filtrate was concentrated till dryness. The crude was purified by flash chromatography (silica, 99:1 cyclohexane:EtOAc) to afford PTH-CN as a white solid (2.40 g, 87% yield). ¹H NMR (300 MHz, CDCl₃): δ 7.51-7.46 (m, 2H), 7.46-7.43 (m, 2H), 7.35-7.31 (m, 2H), 7.30-7.27 (m, 2H), 7.23-7.18 (m, 2H), 7.10-7.04 (m, 2H). Spectroscopic data are in agreement with reported data [50,51].

2.2.2. Synthesis of PTH-COOH

PTH-COOH was synthesized following a previous work [50,51] (see Scheme 1). PTH-CN (2.40 g, 8.0 mmol) was dissolved in 17 mL of an EtOH/H₂O (7:3) mixture. Then, KOH

(6.7 g, 119.4 mmol) was added and the reaction was stirred for 24 h at 100 °C. After cooling, an aqueous solution of HCl (5%) was added to neutralize the reaction. Next, the reaction was poured into 200 mL of water and HCl (conc.) was added until acidic pH. The resulting solid was filtered and washed with copious amounts of water. The white solid, PTH-COOH, was dried under vacuum (2.37 g, 92% yield). ¹H NMR (300 MHz, DMSO-d₆) δ 12.84 (s, 1H), 7.96 (d, *J* = 8.7 Hz, 2H), 7.32 (dd, *J* = 7.6, 1.5 Hz, 2H), 7.22 (d, *J* = 8.7 Hz, 2H), 7.20-7.13 (m, 2H), 7.07 (td, *J* = 7.5, 1.2 Hz, 2H), 6.86-6.80 (m, 2H). Spectroscopic data are in agreement with reported data [50,51].

2.2.3. Synthesis of heterogeneous materials MSN-AP-PTH, MSU-AP-PTH, SBA-15-AP-PTH

First, PTH-COOH (136.0 mg, 0.42 mmol) was dissolved in 40 mL of DMF. Then, *N*-(3-dimethylaminopropyl)-*N*'-ethyl carbodiimide hydrochloride (EDC, 40.0 mg, 0.26 mmol), *N*-hydroxy-succinimide (NHS, 60.0 mg, 0.52 mmol), 2-mercaptoethanol (0.17 mL, 2.42 mmol) and the corresponding functionalized material (MSN-AP, MSU-2-AP and SBA-15-AP, 200.0 mg) were added. The reaction was stirred 24 h at rt and then hydroxylamine hydrochloride (83.0 mg, 2.52 mmol) was added. The resulting white solid was isolated by centrifugation and washed consecutively with DMF (3 x 30 mL) and diethyl ether (3 x 30 mL).

2.3. Compounds and materials characterization

Nuclear magnetic resonance spectra were performed on a Bruker AV-300 spectrometer at 300 MHz for ¹H. ¹H NMR chemical shifts (δ) are reported in ppm relative to the residual peak of the corresponding solvent (CDCl₃ at 7.26 ppm and DMSO-d₆ at 2.50 ppm). Coupling constants are given in Hz. The Solid-State X-Ray Diffraction (XRD) measurements were performed on a X'Pert PRO Panalytical diffractometer, using Cu-Kα

source ($\lambda = 0.154$ nm), and a 2θ range from 5 to 70° (scan step of 5°·min⁻¹). The unit cell (a_o) can be calculated using the following formula:

$$a_o = \frac{2 \cdot d_{hkl}}{\sqrt{3}}$$

IR spectra were acquired on a Thermo Nicolet Avatar 380 FT-IR equipped with a Michelson filter interferometer. For the preparation of the samples, 200 mg of dry KBr were mixed with 2 mg of the sample in a mortar. Pressure was then applied with a hydraulic press until a fine pellet was generated. For the elemental analysis measurements, a LECO CHNS-932 Analyser (Model NO: 601-800-500) was used. UV-visible diffuse reflectance spectroscopy (UV-vis DRS) was carried out on a Shimadzu UV2600 equipment, recording the spectra in the 190–800 nm range using BaSO₄ as reference material. The band gap (E_g) values were obtained from the UV–vis DRS spectra, following the Tauc Plot method [52], considering the photocatalysts as indirect semiconductors. N₂ adsorption–desorption isotherms at -196 °C were obtained in a TriStar 123 equipment (Micromeritics II 3020, Norcross). Solids were outgassed before testing under vacuum at 150 °C for 16 h (VacPrep 60, Micromeritics). Specific surface area (S_{BET}) was calculated using the Brunauer–Emmet–Teller method [53], whereas external surface area (S_{EXT}) and the micropore volume (V_{MP}) were obtained using the *t*-plot method [54] and the microporous surface area (S_{MP}) by difference between S_{BET} and S_{EXT} . The total pore volume (V_T) corresponded to the amount of nitrogen adsorbed at a relative pressure of 0.99. The photoluminescence (PL) spectra of the powder samples were recorded in a Varian Cary Eclipse spectrofluorometer using an excitation wavelength of 325 nm and a sample holder equipped with a quartz window. The Scanning Electron Microscopy (SEM) images were obtained in a Hitachi S-4800 microscope. The Transmission Electron Microscopy (TEM) samples were analysed using a Tecnai F30 (FEI company).

2.4. Photocatalytic performance

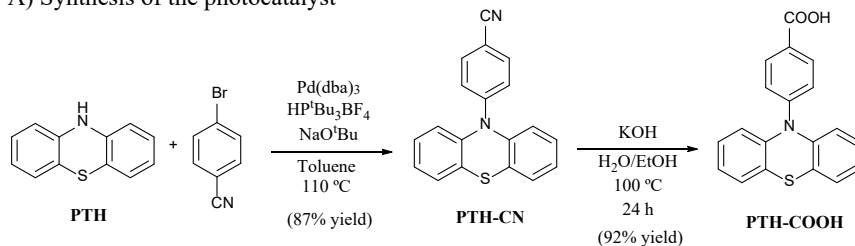
The photocatalytic activity of the different materials was evaluated for the degradation of three model pollutants, acetaminophen (ACE), diclofenac (DCF) and phenol (Ph) under solar-simulated irradiation. A 500 mL Pyrex closed jacketed reactor was placed inside a Suntest XLS+ solar simulator (Atlas), under continuous stirring and controlled temperature (25 °C). The irradiation intensity, provided by a Xe lamp (765–250 W/m²) with a “Daylight” filter (restrains $\lambda \leq 290$ nm), was fixed at 600 W/m² (107.14 klx). In a typical experiment, a photocatalyst amount of 250 mg/L was dispersed in a deionized water solution (150 mL) of the selected target compound with an initial concentration of 10 mg/L at natural pH. The reactor was covered, and the dispersion was maintained under stirring in dark for 16 h with the aim of achieving adsorption equilibrium. Then, the lamp was switched on and the photocatalytic experiment was carried out for 6 h. At different irradiation times, 450 μ L were extracted from the reaction medium and filtered using Whatman 0.2 μ m PTFE syringeless filters (Scharlab). The concentration of the target compounds was analysed with a Shimadzu Prominence-I LC-2030C HPLC (High Performance Liquid Chromatography) equipment, equipped with a diode array detector (SPD-M30A), using a reverse phase C18 column (Eclipse Plus 5 μ m, Agilent). A mixture of acetic acid solution (0.1% v/v)/acetonitrile was used as mobile phase. A gradient 90/10–60/40% method (0.7 mL/min) was used for the quantification of ACE, whereas isocratic methods were applied for the quantification of Ph (50-50%, 0.7 mL/min) and DCF (43-57%, 0.8 mL/min). The detection wavelength used for each compound was fixed to their maximum absorption, being 246, 271 and 276 nm, for ACE, Ph and DCF, respectively. Blank tests were carried out without catalyst at the same reaction conditions to check the stability of the target compounds under solar-simulated irradiation. The experiments were all performed by triplicate.

3. Results and discussion

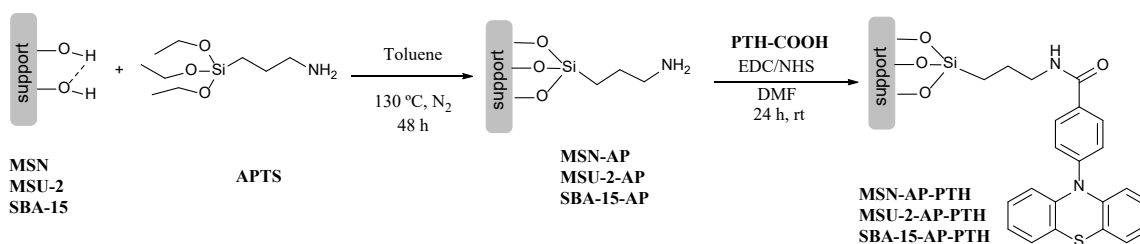
3.1. Synthesis of the materials

The synthesis of MSN-AP-PTH, MSU-AP-PTH and SBA-15-AP-PTH materials was accomplished by covalent bonding of the carboxylated-PTH photocatalyst with the corresponding silica material through an aminopropyl linker, following a post-functionalization strategy. Firstly, PTH photocatalyst containing a carboxylic group was synthesized in two steps starting from phenothiazine and following a reported procedure (Scheme 1A) [50,51]. In the first step, PTH-CN was prepared in 87% yield through a Buchwald-Hartwig coupling. In this reaction, phenothiazine (PTH) is coupled with *p*-bromobenzonitrile in refluxing toluene using Pd₂(dba)₃ as catalyst, ligand HP^tBu₃BF₄ and NaO^tBu as base. Then, the hydrolysis of the nitrile group of PTH-CN was performed by using KOH in a mixture of H₂O/EtOH, obtaining PTH-COOH in high yield. On the other hand, MSN, SBA-15 and MSU-2 silica-based materials were prepared following reported procedures and the characterization data of such materials were in full agreement with the data described in the literature (see Supplementary Material) [46-48]. Each MS material was functionalized with (3-aminopropyl) triethoxysilane (APTS) to incorporate aminopropyl (AP) groups as linkers for anchoring PTH-COOH (Scheme 1B). AP groups were successfully added onto mesoporous silica by heating APTS and the corresponding silica material in toluene at 130 °C. The incorporation of AP onto the material was confirmed by Infrared spectroscopy (IR) due to the presence of the N-H/C-H stretching vibration bands at around 3000 cm⁻¹ (Fig. S1 and Fig. S2 in Supplementary Material), as previously reported [49]. Finally, the photocatalyst was anchored to the silica via chemical bond between the AP groups of the material and the carboxylic acid of PTH-COOH using EDC and NHS as coupling reagents [41].

A) Synthesis of the photocatalyst **PTH-COOH**



B) Synthesis of materials



Scheme 1. A) Synthesis of the photocatalyst PTH-COOH; B) Synthesis of MSN-AP-PTH, MSU-AP-PTH and SBA-15-AP-PTH materials.

3.2. Characterization of the materials

The characterization of the three newly synthesized photocatalytic mesoporous silica materials was performed using a combination of IR analysis, solid-state X-ray diffraction (XRD), porosity and microscopy (SEM and TEM) techniques. The IR analysis of the PTH-anchored materials showed the characteristic Si-OH (750 cm^{-1}), Si-O-Si (1000 cm^{-1}) and O-H (3500 cm^{-1}) stretching bands of the silica-structure, the C-H/N-H stretching band (3000 cm^{-1}) of the aminopropyl linker and the appearance of a band at $\sim 1650\text{ cm}^{-1}$, which corresponds to the C=O stretching of the amide bond (Fig. 2 and Fig. S1-S2 of Supplementary Material). The latter band confirmed the tethering of the PTH photocatalyst into the material. In addition, the absence of the COOH vibration (strong band at $\sim 3000\text{ cm}^{-1}$) in the IR spectra excludes the adsorption of PTH-COOH inside the silica support. The XRD technique allowed to identify the mesoscopic structure of the PTH-functionalized silica materials and compared with that of the precursor materials (MSN, SBA-15 and MSU-2). As shown in Fig. 3, MSN and SBA-15 presents three peaks that

correspond to the Miller planes (100), (110), and (200), which are ascribed to a hexagonal mesoscopic order, while MSU-2 has a worm-hole distribution of the pores, ascribed to the plane (110) [55]. In the MSN-AP-PTH, MSU-AP-PTH and SBA-15-AP-PTH materials, the XRD patterns of the corresponding MS are maintained (see for instance the distance of the (100) plane in Table 1) but a reduction of the diffraction peaks intensity was observed, indicating the PTH functionalization within the pores. Those data are also in agreement with the reduction of unit cell parameter (a_o) after functionalization (Table 1).

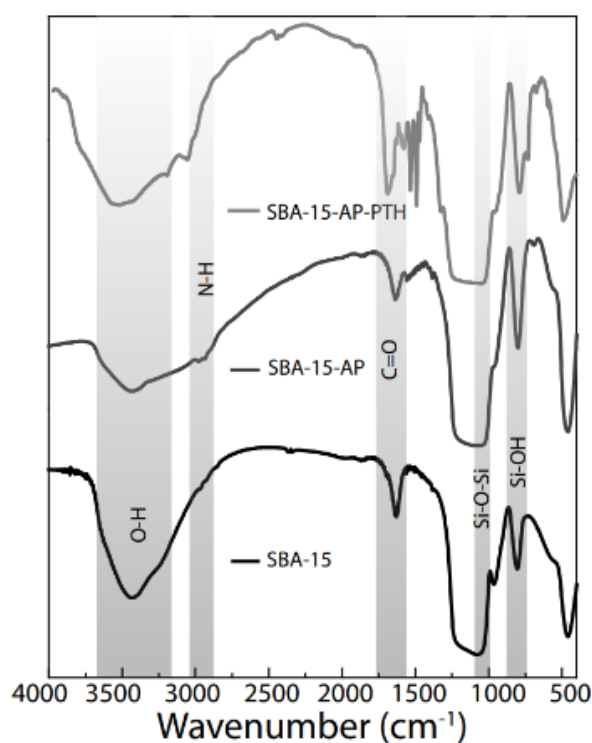


Figure 2. IR spectra of SBA-15, SBA-15-AP and SBA-15-AP-PTH.

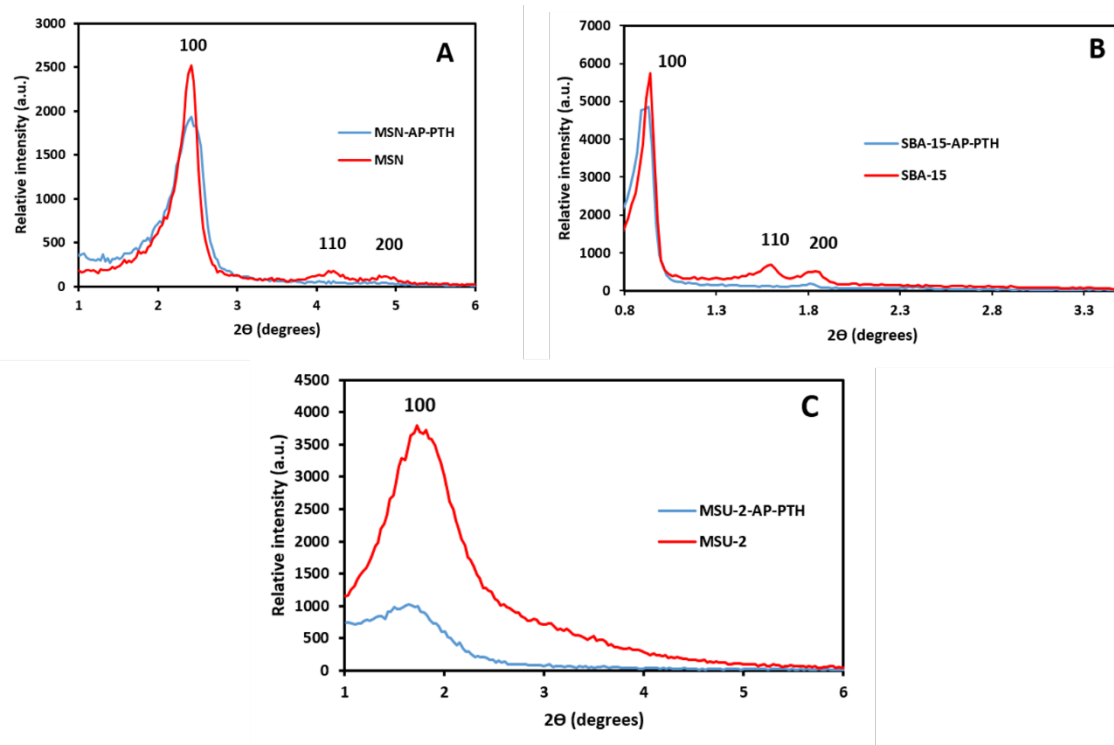


Figure 3. Powder XRD patterns of mesoporous silicas: A) MSN and MSN-AP-PTH, B) SBA-15 and SBA-15-AP-PTH, C) MSU-2 and MSU-2-AP-PTH.

Table 1. Structural, textural and composition parameters of the mesoporous silica supports and the functionalized materials.

Sample	d_{100} (Å) ^a	a_o (Å) ^b	S_{BET} ^c (m ² ·g ⁻¹)	S_{MP} ^d (m ² ·g ⁻¹)	S_{EXT} ^d (m ² ·g ⁻¹)	V_{MP} ^e (cm ³ ·g ⁻¹)	V_T ^e (cm ³ ·g ⁻¹)	S (wt%)	PTH Content ^f (mmoles·g ⁻¹)
SBA-15	96.25	111.14	757	167	590	0.063	0.994	-	-
SBA-15-AP-PTH	95.82	110.64	125	12	113	0.003	0.185	1.26	0.394
MSN	36.50	42.15	771	190	581	0.127	0.662	-	-
MSN-AP-PTH	37.96	43.80	69	16	53	0.007	0.207	1.25	0.391
MSU-2	52.04	60.09	950	441	509	0.404	0.822	-	-
MSU-2-AP-PTH	51.55	59.52	411	145	266	0.057	0.213	1.71	0.534

^a Miller plane (100) distance. ^b a_o : unit cell; $a_o = 2 \cdot d_{110} / \sqrt{3}$. ^c S_{BET} : specific surface area. ^d S_{MP} and S_{EXT} : microporous and non-microporous surface area, respectively. ^e V_{MP} and V_T : micropore and total volume, respectively. ^f Calculated according to the S content by CHNS elemental analysis.

The N₂ adsorption–desorption isotherms at -196 °C of the different silica precursors and their functionalized materials are showed in Fig. 4. The characteristic parameters of their porous textures are summarized in Table 1. SBA-15 exhibits a type IV isotherm according to the IUPAC classification [56], characteristic of a mesoporous material with a significant micropore contribution and high surface area (Table 1). This isotherm describes a H1 hysteresis loop typical of materials with a cylindrical pore geometry and a high degree of pore size uniformity [55]. These textural properties are due to the hexagonal arrangement of pores characteristic of SBA-15 that generate 2-D longitudinally oriented tubular pores. On the other hand, MSN displays an isotherm between type IV and VI proper of an ordered mesoporous material. This porous structure is due to a hexagonal arrangement of the pores yielding to silica spheres. MSN isotherm also describes two sharp increases in the volume adsorbed in the ranges 0.2-0.4, and 0.8-1.0 of P/P₀, due to capillary condensation of nitrogen into the straight pores of the material [57,58]. MSU-2 presents a type IV isotherm, characteristic of a mesoporous material, with some contribution of micropores, as revealed the nitrogen adsorption at low relative pressures. This isotherm also displays a small hysteresis loop between the relative pressures of 0.3 and 0.8, due to the capillary condensation of nitrogen, as previously mentioned. The functionalization of all silica supports significantly reduces their porosity, as suggested by the reduction in the nitrogen volume adsorbed (Fig. 4). Moreover, the loss of porosity after grafting is evident in the values of the textural parameters (Table 1), since BET surface area and pore volume of SBA-15, MSN and MSU-2 are greatly reduced after the functionalization with AP and PTH.

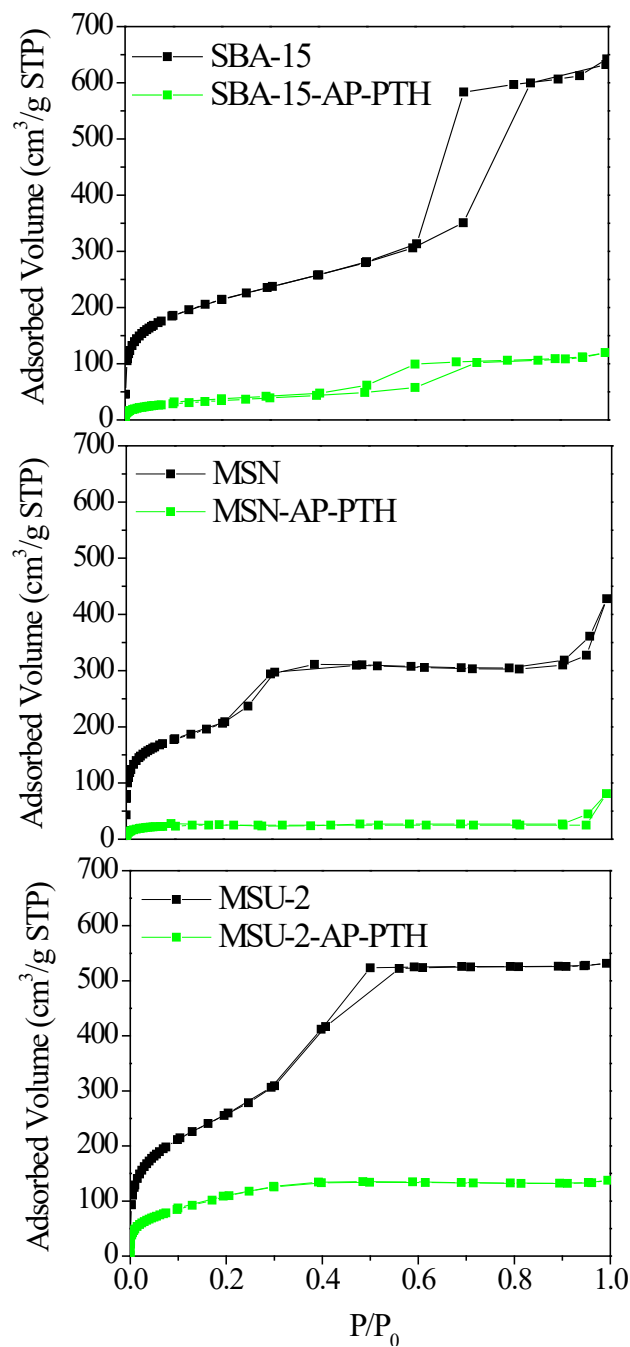
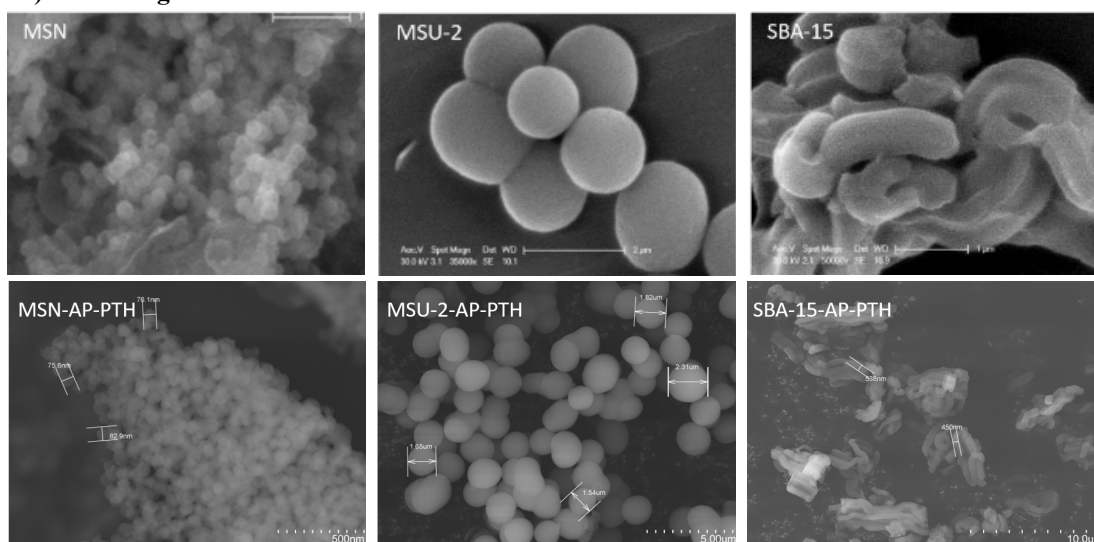


Figure 4. Nitrogen adsorption–desorption isotherms at -196 °C of the silica supports (black colour) and the functionalized materials (green colour).

The morphology of the PTH-supported materials was analysed by SEM and TEM. The images of the supported materials corroborated that the morphology, particle size and pore arrangement was unmodified during the functionalization processes (see and compare top

and bottom A and B, Fig. 5). Finally, the PTH content of the three different MS samples was determined by elemental analysis (Table 1). MSU-2 material exhibited higher PTH loading (1.71% S content) compared with those of SBA-15 and MSN (1.25-1.26% S content).

A) SEM images



B) TEM images

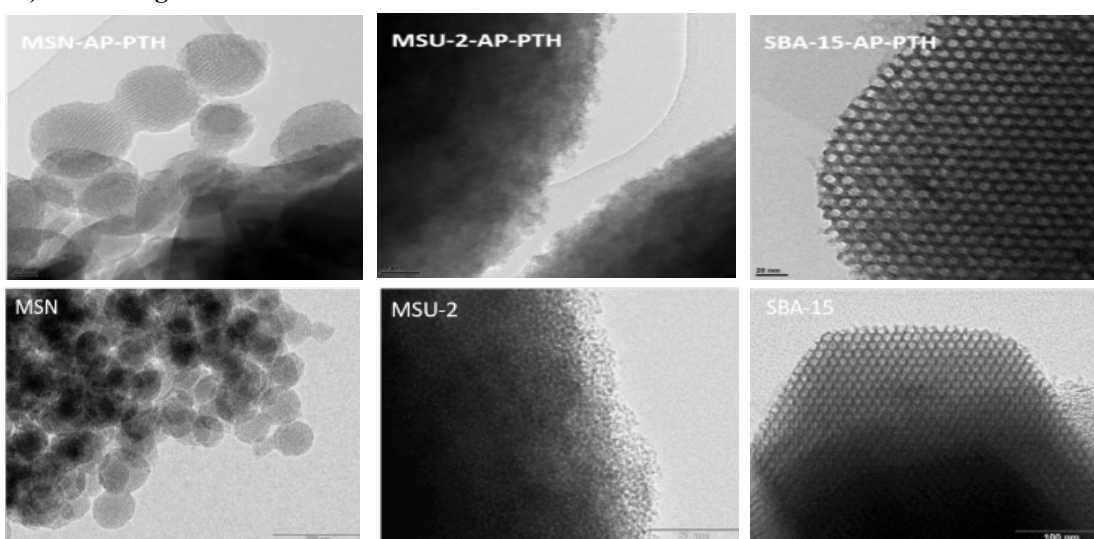


Figure 5. A) SEM images of the three unfunctionalized (up, Scale: 1 μm for SBA-15 and MSN, 2 μm for MSU-2) and PTH-supported materials (bottom, Scale: 500 nm for MSN-AP-PTH, 5 μm for MSU-2-AP-PTH and 10 μm for SBA-15-AP-PTH). B) TEM images of the three unfunctionalized (up, 200 nm for MSN-AP-PTH, 50 nm for MSU-2-AP-PTH

and 100 nm for SBA-15-AP-PTH) and PTH-supported materials (bottom, 20 nm for MSN-AP-PTH, 50 nm for MSU-2-AP-PTH and 20 nm for SBA-15-AP-PTH).

The UV-visible absorbance spectra of the functionalized materials are depicted in Fig. 6A. Since the silica supports have negligible light absorption in the UV-vis range (spectra not shown), the absorption bands observed at 212, 257 and 316 nm are due to the PTH grafted to the support. The two bands at lower wavelength values correspond to the π - π^* transitions, while the band at 316 nm was assigned to a n - π^* transition [59]. The band gap values (E_g) were calculated by the Tauc Plot method, analysing the linear relationship between $(\alpha h\nu)^{1/2}$ and photon energy ($h\nu$) (Fig. 6B). The E_g values are obtained from the intercept of the extrapolation of the linear branch with the base line (background). All functionalized materials have similar band gap values close to 3.3 eV. Since the absorption branch is due to the phenothiazine grafted over the silica support, it was expected that all functionalized materials have similar absorption spectra and, thus, band gap values.

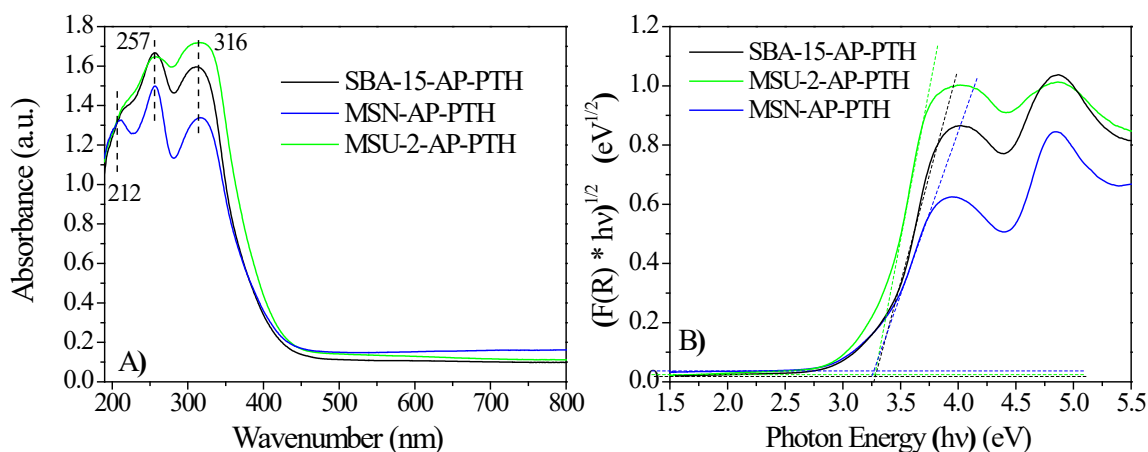


Figure 6. A) UV-vis diffuse absorbance spectra, and B) Tauc plots of the functionalized materials.

In order to further investigate the optical properties of the functionalized materials, the photoluminescence (PL) spectra were measured (Fig. 7). PL can be used to analyse charge

carrier recombination and are independent of the excitation wavelength (Kasha rule) [50]. As shown in the UV-vis absorption spectra, all samples exhibit an excellent ability to absorb energy in UV-vis extent (Fig. 6) and they have also strong fluorescence emission intensity in blue range due to the characteristic π - π^* transition of the PTH (Fig. 7). SBA-15-AP-PTH displays a broad band with a maximum at 488 nm that slightly shifts to higher wavelengths for the other materials. It is well-known that the differences in the structures of mesoporous materials can induce changes in energy absorption and fluorescence emission. This bathochromic shift in the blue emission spectra of guest molecules supported on inorganic materials, such as mesoporous silica, depends on the pore size and has been attributed to the orbital-confinement effect of the inorganic material [41,61]. This confinement effect generates an overall reduction of the HOMO-LUMO energy gap of the guest molecule and, consequently, shifts the emission band at higher wavelengths [41,61]. Moreover, it has been reported that the intensity of the PL spectra is directly related with the charge recombination rate, thus a reduction of the luminescence intensity indicates a lower recombination [62]. In this study, SBA-15-AP-PTH undergoes the highest recombination rate, whereas MSN-AP-PTH yields the lowest one.

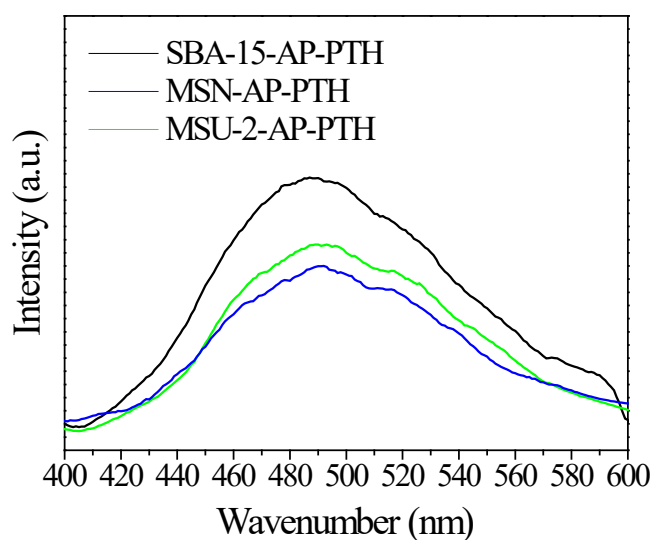


Figure 7. Photoluminescence spectra (PL) of the functionalized materials.

3.3. Photocatalytic degradation of pollutants using solar light

The photocatalytic performance of functionalized materials was initially tested in the degradation of acetaminophen (ACE) under solar light irradiation. Experiments were carried out in the absence of photocatalyst (photolysis blank test) and with the bare-silica precursors (not functionalized), verifying, in all cases, that the ACE concentration did not vary through the reaction (results not shown). This fact confirms that ACE is stable under solar light and that the silica precursors are not photoactive in this reaction. Moreover, the amount of ACE adsorbed on the different photocatalysts without light irradiation (in dark) is negligible despite the differences in porosity of the photocatalysts. The evolution of the ACE concentration with irradiation time is shown in Fig. 8 for all functionalized materials. SBA-15-AP-PTH shows a significantly higher activity than the other functionalized materials, yielding a conversion close to 70% after 6 h of reaction. As previously mentioned, SBA-15-AP-PTH showed the highest recombination rate (Fig. 7), which can be indicative of higher photogeneration of electron-hole pairs, and thus, a better ACE photodegradation. On the other hand, the ACE removal follows quite well a pseudo-first order kinetic. The values of the corresponding rate constant, k , are depicted in Fig. 8B. The highest value achieved by SBA-15-AP-PTH, 0.42 h^{-1} , is similar to those previously reported by our research group for the ACE degradation with TiO_2 /activated carbon heterostructures (ca. 0.50 h^{-1}) [63] and significantly higher than that reported when using ZnO /sepiolite photocatalyst [64]. It is important to highlight that attempts to photodegrade ACE using homogeneous PTH (non-supported photocatalyst) were unsuccessful in water media. This observation is in agreement with previously reported studies which shown that the emission of planar phenoxazine and phenothiazine derivatives is quenched when intermolecular π - π stacking interactions take place in aggregation states [65-66]. Such

effect, known as aggregation-cause quenching, has limited the application of homogeneous PTH derivatives in aqueous media due to the aggregation provoke by their hydrophobic structure. However, the results presented in this work revealed the promising activity of the phenothiazine dye grafted on a mesoporous silica for the removal of pollutants in wastewater.

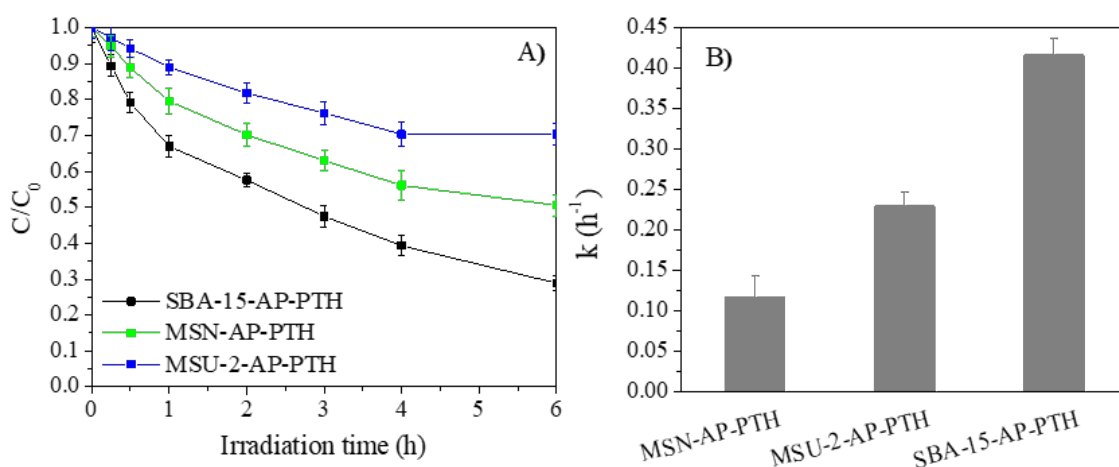


Figure 8. A) Time-course of acetaminophen concentration under solar irradiation using the functionalized materials (250 mg/L of the corresponding photocatalyst; initial ACE concentration: 10 mg/L; intensity of irradiation: 600 W/m²); B) Apparent first order rate constants (k) for ACE disappearance with functionalized materials. Error bars represent standard deviation based on triplicate measurements.

Since the SBA-15-AP-PTH was the most active photocatalyst for ACE removal, further photocatalytic experiments were performed exclusively with this photocatalyst. In those experiments two other target compounds were studied, selecting diclofenac (DCF) as another example of emerging contaminant and phenol (Ph) as example of priority contaminant. Fig. 9A depicts the evolution of the concentration of the contaminants upon reaction with SBA-15-AP-PTH, whereas Fig. 8B shows the corresponding kinetic

constants. DCF was easily degraded, yielding conversion values close to 90% after 4 h and a high-rate constant, while Ph almost remained unmodified, just achieving 20% of conversion. This behaviour may easily be explained considering the interactions between the photocatalytic material and the contaminants. We have previously described that catalysts supported on this type of silica are able to discriminate compounds by polarity, increasing the reaction rate of those substrates [41]. Based on this study, we propose that the more polar the compound is, the faster is its degradation, since the interaction of the polar silica material with the pollutant by hydrogen bonds will be favoured. On account of this, DCF, having amine and acid groups, is the most polar compound (Fig. 9C), which is in agreement with its faster degradation. By contrast, the less polar compound, phenol (Ph), was the less degraded pollutant. Therefore, DCF molecules may have a stronger interaction with surface of SBA-15-AP-PTH by hydrogen bond interactions and electronic attractions, boosting and facilitating its photodegradation.

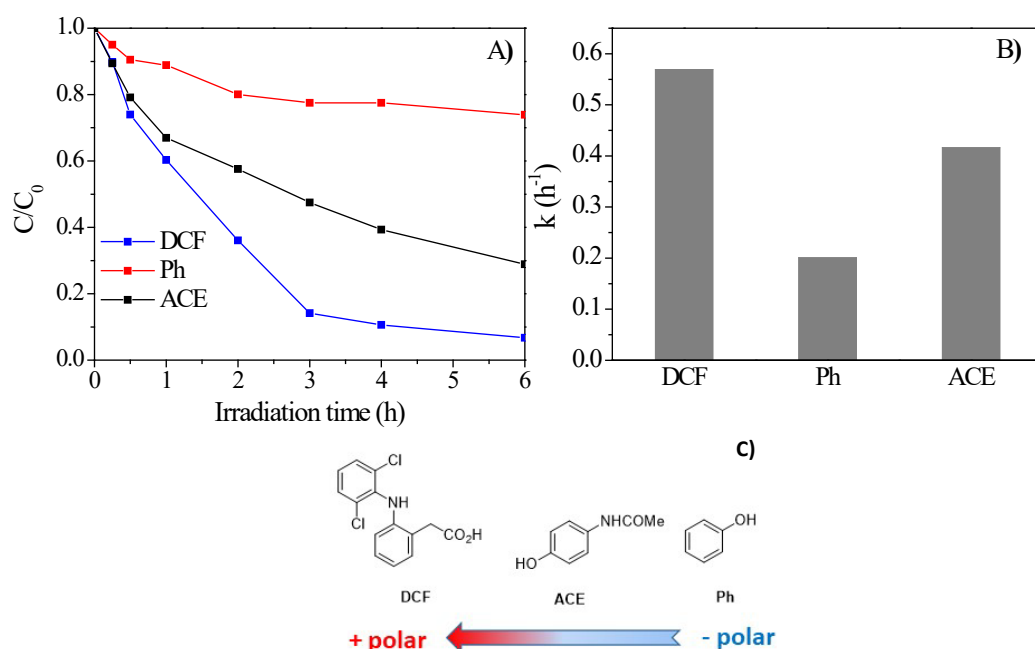


Figure 9. A) Time-course of ACE, DCF and Ph concentrations under solar irradiation (250 mg/L of SBA-15-AP-PTH; initial DCF/Ph concentration: 10 mg/L; intensity of irradiation:

600 W/m²); B) Apparent first order rate constant (k) for ACE, DCF and Ph disappearance with SBA-15-AP-PTH. C) Chemical structure of the compounds degraded in this study.

4. Conclusions

In summary, we have demonstrated that the anchoring of an organic photocatalyst, such PTH, into mesoporous silica material is an ideal approach for obtaining active catalyst for the degradation of pollutants in water, overcoming the disadvantages of the organic catalysts in such media. The synthesis of the three different heterogeneous photocatalysts follows an easy and straightforward synthesis. The characterization of the materials showed that PTH was covalently bonded into the pores and its optical properties are maintained after the immobilization. The best catalytic performances were obtained using PTH anchored into SBA-15 material, which is able to efficiently degraded contaminants such as diclofenac and acetaminophen.

Acknowledgements

Financial support was provided by the European Research Council (ERC-CoG, contract number: 647550), Spanish Government (RTI2018-095038-B-I00), and Spanish State Research Agency (PID2019-106186RB-I00/AEI/10.13039/ 501100011033).

Appendix A. Supplementary material

Supplementary material is provided in a word file.

References

- [1] C.K. Prier, D.A. Rankic, D.W.C. MacMillan. Chem. Rev. 113 (2013) 5322-5363.
- [2] D.M. Schultz, T.P. Yoon. Science 343 (2014) 985-995.

- [3] K. Perovic, F.M. dela Rosa, M. Kovacic, H. Kusic, U.L. Stangar, F. Fresno, D.D. Dionysiou, A.L. Bozic. *Materials* 13 (2020) 1338-1382.
- [4] A. Kumar, M. Khan, J. He, I.M.C. Lo. *Water Res.* 170 (2020) 115356-115374.
- [5] A.S. Hart, C. Bikram, N.K. Subbaiyan, P.A. Karr, F.D'Souza. *App. Mater. Interfaces* 4 (2012) 5813-5820.
- [6] S. Agrawal, M. Pastore, G. Marotta, M.A. Reddy, M. Chandrasekharam, F. De Angelis. *J. Phys. Chem.* 117 (2013) 9613-9622.
- [7] B.N. DiMarco, R.M. O'Donnell, G.J. Meyer. *J. Phys. Chem. C.* 119 (2015) 21599-21640.
- [8] S. Yellappa, W.A. Webre, H.B. Gobeze, A. Middleton, C.B. KC, F. D'Souza. *ChemPlusChem* 82 (2017) 896-903.
- [9] J. Lee, J. Kwak, K.C. Ko, J.H. Park, J.H. Ko, N. Park, E. Kim, D.H. Ryu, T.K. Ahn, J.Y. Lee, S.U. Son. *Chem. Commun.* 48 (2012) 11431-11433.
- [10] M. Watanabe, H. Hagiwara, A. Iribe, Y. Ogata, K. Shiomi, A. Staykov, S. Ida, K. Tanaka, T. Ishihara. *J. Mater. Chem. A.* 2 (2014) 12952-12961.
- [11] B. Cecconi, N. Manfredi, R. Ruffo, T. Montini, I. Romero-Ocaña, P. Fornasiero, A. Abbotto. *ChemSusChem* 8 (2015) 4216-4228.
- [12] N. Manfredi, B. Cecconi, V. Calabrese, A. Minotti, F. Peri, R. Ruffo, M. Monai, I. Romero-Ocaña, T. Montini, P. Fornasiero, A. Abbotto. *Chem. Commun.* 52 (2016) 6977-6980.
- [13] N. Mandredi, M. Monai, T. Montini, M. Salamone, R. Ruffo, P. Fornasiero, A. Abbotto. *Sustain. Energ. Fuels* 1 (2017) 694-698.
- [14] N. Manfredi, M. Monai, T. Montini, F. Peri, F. De Angelis, P. Fornasiero, A. Abbotto. *ACS Energy Lett.* 3 (2018) 85-91.

- [15] O. Suryani, Y. Higashino, H. Sato, Y. Kubo. *ACS Appl. Energ. Mater.* 2 (2019) 448-458.
- [16] F. Speck, D. Rombach, H.-A. Wagenknecht. *Beilstein J. Org. Chem.* 15 (2019) 52–59.
- [17] A. J. Boyington, C.P. Seath, A.M. Zearfoss, Z. Xu, N.T. Jiu. *J. Am. Chem. Soc.* 141 (2019) 4147-4153.
- [18] A.M. Martínez-Gualda, R. Cano, L. Marzo, R. Pérez-Ruiz, J. Luis-Barrera, R. Mas-Ballesté, A. Fraile, V.A. de la Peña O’Shea, J. Alemán. *Nat. Commun.* 10 (2019) 2634.
- [19] J.H. Park, K.C. Ko, E. Kim, N. Park, J.H. Ko, D.H. Ryu, T.K. Ahn, J.Y. Lee, S.U. Son. *Org. Lett.* 14 (2012) 5502-5505.
- [20] S. Li, W. Zhang, S. Yang, F. Chen, C. Pan, J. Tang, K.A.I. Zhang, G. Yu. *Chem. Eng. J.* 408 (2021) 127261.
- [21] E.H. Discekici, N.J. Treat, S.O. Poelma, K.M. Mattson, Z.M. Hudson, Y. Luo, C.J. Hawker, J.R. de Alaniz. *Chem. Commun.* 51 (2015) 11705-11708.
- [22] S.O. Poelma, G.L. Burnett, E.H. Discekici, K.M. Mattson, N.J. Treat, Y. Luo, Z.M. Hudson, S.L. Shankel, P.G. Clark, J.W. Kramer, C.J. Hawker, J.R. de Alaniz. *J. Org. Chem.* 81 (2016) 7155-7160.
- [23] M. Pelaez, N.T. Nolan, S.C. Pillai, M.K. Seery, P. Falaras, A.G. Kontos, P.S.M. Dunlop, J.W.J. Hamilton, J.A. Byrne, K. O’Shea, M.H. Entezari, D.D. Dionysiou. *Appl. Catal. B Environ.* 125 (2012) 331–349.
- [24] K.P. Gopinath, N.V. Madhav, A. Krishnan, R. Malolan, G. Rangarajan. *J. Environ. Manage.* 270 (2020) 110906.
- [25] A. Di Paola, E. García-López, G. Marci, L. Palmisano. *J. Hazard. Mater.* 211–212 (2012) 3–29.
- [26] M.D. Regulacio, M.-Y. Han. *Acc. Chem. Res.* 49 (2016) 511–519.

- [27] S. Cao, J. Low, J. Yu, M. Jaroniec. *Adv. Mater.* 27 (2015) 2150–2176.
- [28] J. Fu, J. Yu, C. Jiang, B. Cheng. *Adv. Energy Mater.* 8 (2018) 1701503.
- [29] Y. Li, X. Li, H. Zhang, J. Fan, Q. Xiang. *J. Mater. Sci. Technol.* 56 (2020), 69-88.
- [30] C. Belver, J. Bedia, A. Gomez-Aviles, M. Peñas-Garzon, J.J. Rodriguez. In *Nanoscale materials in water purification*, S. Thomas, D. Pasquini, S.Y. Leu, D.A. Gpakumar, Ed., Elsevier, Amsterdam (2019) pp. 581–650.
- [31] J. Bedia, V. Muelas-Ramos, M. Peñas-Garzón, A. Gómez-Avilés, J.J. Rodríguez, C. Belver. *Catalysts* 9 (2019) 52.
- [32] V. Hasija, P. Raizada, A. Sudhaik, P. Singh, V.K. Thakur, A. A. P. Khan. *Solid State Sci.* 100 (2020) 106095.
- [33] N. Chandel, K. Sharma, A. Sudhaik, P. Raizada, A. Hosseini-Bandegharai, V.K. Thakur, P. Singh. *Asian J. Chem.* 13 (2020), 4324-4340.
- [34] F. Hoffmann, M. Cornelius, J. Morell, M. Fröba. *Angew. Chem. Int. Ed.* 45 (2006) 3216-3251.
- [35] C. Perego, R. Millini. *Chem. Soc. Rev.* 42 (2013) 3956-3976.
- [36] N. Pal, A. Bhaumik. *RSC Adv.* 5 (2015) 24363-24391.
- [37] A. Jana, J. Mondal, P. Borah, S. Mondal, A. Bhaumik, Y. Zhao. *Chem. Commun.* 51 (2015) 10746–10749.
- [38] K. Mori, M. Tottori, K. Watanabe, M. Che, H. Yamashita. *J. Phys. Chem. C.* 115 (2001) 21358–21362.
- [39] K. Feng, R.-Y. Zhang, L.-Z. Wu, B. Tu, M.-L. Peng, L.-P. Zhang, D. Zhao, C.-H. Tung, J. Am. Chem. Soc. 128 (2006) 14685–14690.
- [40] K. Mori, K. Watanabe, M. Kawashima, M. Che, H. Yamashita. *J. Phys. Chem. C.* 115 (2001) 1044–1050.

- [41] D. González-Muñoz, A. Casado-Sánchez, I. del Hierro, S. Gómez-Ruiz, S. Cabrera, J. Alemán. *J. Catal.* 373 (2019) 374-383.
- [42] B. Castanheira, F.J. Trindade, L. dos Santos Andrade, I.L. Nantes, M.J. Politi, E.R. Triboni, S. Brochsztain. *J. Photochem. Photobiol. A Chem.* 332 (2017) 316-325.
- [43] A.W. Franz, Z. Zhou, R. Turdean, A. Wagener, B. Sarkar, M. Hartmann, S. Ernst, W.R. Thiel, T.J.J. Müller. *Eur. J. Org. Chem.* (2009) 3895–3905.
- [44] Z. Zhou, A.W. Franz, S. Bay, B. Sarkar, A. Seifert, P. Yang, A. Wagener, S. Ernst, M. Pagels, T.J.J. Müller, W.R. Thiel. *Chem. Asian J.* 5 (2010) 2001-2015.
- [45] M. Hemgesberg, B. Bayarmagnai, N. Jacobs, S. Bay, S. Follmann, C. Wilhelm, Z. Zhou, M. Hartman, T.J.J. Müller, S. Ernst, G. Wittstock, W.R. Thiel. *RSC Adv.* 3 (2013) 8242–8253.
- [46] Y. Zhao, B. Trewyn, I. Slowing, V. Lim. *J. Am. Chem. Soc.* 131 (2009) 8398-8400.
- [47] D. Zhao, Q. Huo, J. Feng, B. Chmelka, G. Stucky. *J. Am. Chem. Soc.* 120 (1998) 6024–6036.
- [48] D. Pérez-Quintanilla, A. Sánchez, I. Hierro, M. Fajardo, I. Sierra. *J. Nanosci. Nanotechnol.* 9 (2009) 4901–4909.
- [49] R. Kotcherlakota, A. K. Barui, S. Prashar, M. Fajardo, D. Briones, A. Rodríguez-Diéguez, C. R. Patra, S. Gómez-Ruiz. *Biomater. Sci.* 4 (2016) 448-459.
- [50] Y. S. Park, J. Choi, D. Kim, B. Lee, H. Suh, J.H. Kim. *Mol. Cryst. Liq. Cryst.* 550 (2011) 294–303.
- [51] J. Yang, Z. Ren, B. Chen, M. Fang, Z. Zhao, B.Z. Tang, Q. Peng, Z. Li. *J. Mater. Chem. C* 5 (2017) 9242-9246.
- [52] J. Tauc. *Mater. Res. Bull.* 5 (1970) 721–729.
- [53] S. Brunauer, P.H. Emmett, E. Teller. *J. Am. Chem. Soc.* 60 (1938) 309–319.
- [54] B.C. Lippens, J.H. De Boer. *J. Catal.* 4 (1965) 319–323.

- [55] K.S.W. Sing. *Pure Appl. Chem.* 57 (1985) 603–619.
- [56] M. Kruk, M. Jaroniec. *Chem. Mater.* 13 (2001) 3169–3183.
- [57] D. Díaz-García, P.R. Ardiles, S. Prashar, A. Rodríguez-Diéguez, P.L. Páez, S. Gómez-Ruiz. *Pharmaceutics* 11 (2019) 30.
- [58] D. Díaz-García, L. Sommerova, A. Martisova, H. Skoupilova, S. Prashar, T. Vaculovic, V. Kanicky, I. Hierro, R. Hrstka, S. Gómez-Ruiz. *Micropor. Mesopor. Mater.* 300 (2020) 110154.
- [59] L. Piñero, X. Calderón, J. Rodríguez, I. Nieves, R. Arce, C. García, R. Oyola, J. Photochem. Photobiol. A Chem. 198 (2008) 85-91.
- [60] M. Kasha. *Disc. Faraday. Soc.* 9 (1950) 14–19.
- [61] F. Márquez, V. Martí, E. Palomares, H. García, W. Adam. *J. Am. Chem. Soc.* 124 (2002) 7264-7265.
- [62] T. Kircherts, J.A. Márquez, M. Stolterfoht. *T. Unold. Adv. Energy Mater.* 10 (2020) 1904134.
- [63] M. Peñas-Garzón, A. Gomez-Aviles, C. Belver, J.J. Rodriguez, J. Bedia. *Chem. Eng. J.* 392 (2020) 124867.
- [64] M. Akkari, P. Aranda, C. Belver, J. Bedia, A. Ben Haj Amara, E. Ruiz-Hitzky. *Appl. Clay Sci.* 156 (2018) 104–109.
- [65] M. Huang, H. Lu, K. Wang, B. Liu, M. Wang, X. Qiao, J. Yang. *Dyes Pigm.* 186 (2021) 108992.
- [66] A. Ghanadzadeh Gilani, Z. Poormohammadi-Ahandani, R. Kia. *Spectrochim. Acta A Mol. Biomol. Spectrosc.* 189 (2018) 543-555.